Open Access on 05/03/2015

Kinetics of DNA Tile Dimerization

Shuoxing Jiang, Hao Yan, and Yan Liu*

Department of Chemistry and Biochemistry and Biodesign Institute, Arizona State University, Tempe, Arizona 85287, United States

ABSTRACT Investigating how individual molecular components interact with one another within DNA nanoarchitectures, both in terms of their spatial and temporal interactions, is fundamentally important for a better understanding of their physical behaviors. This will provide researchers with valuable insight for designing more complex higher-order structures that can be assembled more efficiently. In this report, we examined several spatial factors that affect the kinetics of bivalent, double-helical (DH) tile dimerization, including the orientation and number of sticky ends (SEs), the flexibility of the double helical domains, and the size of the tiles. The rate constants we obtained confirm our hypothesis that increased nucleation opportunities and well-aligned SEs accelerate tile−tile dimerization. Increased flexibility in the tiles causes slower dimerization rates, an effect that can be reversed by introducing restrictions to the tile flexibility. The higher dimerization rates of more rigid tiles results from the opposing effects of higher activation energies and higher pre-exponential factors from the Arrhenius equation, where the pre-exponential factor dominates. We believe that the results presented here will assist in improved implementation of DNA tile based algorithmic self-assembly, DNA based molecular robotics, and other specific nucleic acid systems, and will provide guidance to design and assembly processes to improve overall yield and efficiency.

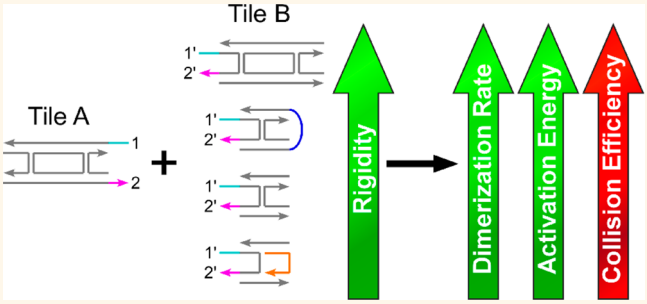

KEYWORDS: DNA tile dimerization · bivalent sticky end association · dimerization kinetics · DNA tile flexibility · dynamic DNA nanostructures

In recent years, DNA has emerged as an attractive building material for creating complex architectures at the nanometer scale that simultaneously affords versatility and modularity.[1−5] This is due to a number of favorably distinct features of DNA, for example: the reliability of base-pair interactions, the availability of DNA manipulation techniques, and the ease and affordability of custom oligonucleotide synthesis. New design strategies have evolved to enrich the collection of two- and three-dimensional DNA nanostructures,[6−10] and spatial and/or temporal manipulation of molecules displayed from DNA scaffolds have been demonstrated.[11−13] With the expanding complexity and functionality of DNA toolboxes, a quantitative understanding of the dynamics of DNA self-assembly, and identification of those factors that influence the kinetics, will provide researchers with more subtle design guidelines that facilitate more precise spatial and temporal control.

The kinetics of single-stranded DNA (ssDNA) hybridization has been thoroughly investigated in the past decades.[14−22] For example, a typical bimolecular rate constant for ssDNA binding to its complementary strand is on the order of $\sim 1.0 \times 10^6\ M^{-1} \cdot s^{-1}$.[14] We recently showed that the bimolecular rate constant for ssDNA hybridization to a 20-nucleotide (nt) probe extended from a multihelical DNA tile is $(1.04 \pm 0.05) \times 10^6\ M^{-1} \cdot s^{-1}$,[19] consistent with the association rate of complementary ssDNA strands. The factors that affected the hybridization rate included the position from which the probe was displayed, the steric crowding in the vicinity of the probe, and the sequences flanking the hybridization domain. Despite the continued interest and effort put toward constructing more complex structural motifs, there are very few other reports describing the kinetic behavior of multivalent DNA architectures. In this work we study the kinetics of DNA tile−tile association.

DNA tiles, or branched DNA motifs, generally carry multiple single-stranded overhangs called "sticky end" (SE) that allow them to be linked together into 1D or 2D arrays. Holliday-junction (HJ) and double-crossover (DX) tiles are among the first and simplest DNA tiles that were constructed, and they are also the most common structural motifs used in DNA based assembly. HJ tiles have a flexible junction domain and

* Address correspondence to yan_liu@asu.edu.

Received for review February 5, 2014 and accepted May 3, 2014.

Published online May 03, 2014
10.1021/nn500721n

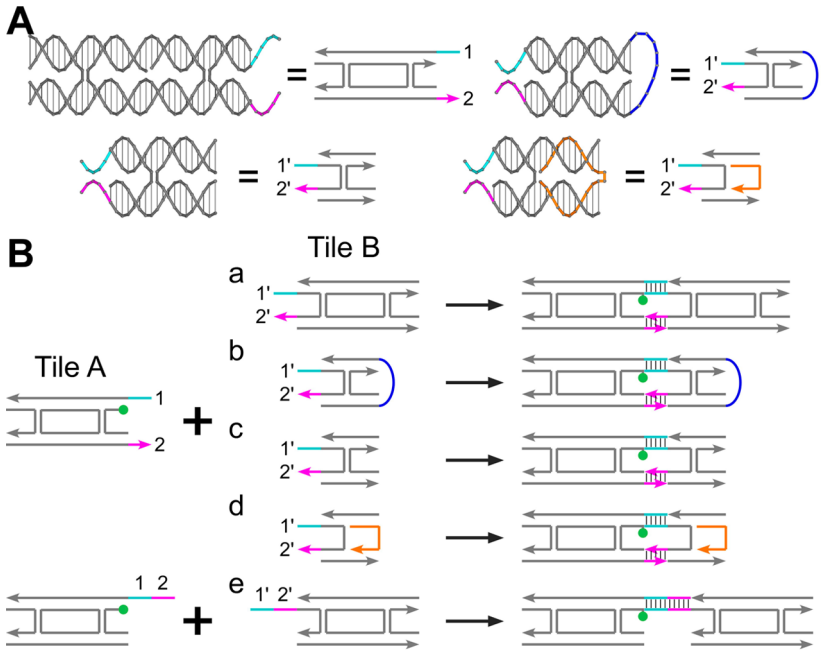

Figure 1. (A) Helical arrangements of rigid, semirigid, and flexible tiles in this study. (B) Schematic designs of rigid, semirigid, and flexible tile pairs in this study include (a) DAE homodimer, and heterodimers of a DAE tile with (b) a tethered-junction tile, (c) a HJ tile, and (d) a meso-junction tile; the second tile flexibility increases from (a) to (d). A reporter fluorophore (green dot: 6-FAM) was introduced to the DAE tile at the interface between the tiles. (e) DAE homodimer with a single 10-nt SE. This homodimer was evaluated for quantitative comparison with the assembly through two SEs in (a) to determine the influence of the number of SE interactions.

may carry up to four SEs, while DX tiles are relatively rigid and also carry four SEs.

Subtle variations or modifications are easily introduced to HJ tiles, including changing the number and orientations of the SEs, linking the ends together to generate a tethered-junction, or breaking one of the two connecting strands at the junction point to produce a meso-junction.[23,24] The nonbinding ends of the flexible tiles were extended with multiple thymines to prevent nonspecific tile−tile stacking and to ensure that the flexible tiles all had the same molecular weight. Therefore, this group of simple DNA nanostructures represents an ideal model to comprehensively study the kinetics of multivalent DNA−tile association, where the desired structural features are easily implemented. This study aims to understand the dimerization behavior of pairs of DNA tiles through SE association (either one or two interactions). The results will certainly benefit the design and functionality of dynamic DNA devices.

RESULTS AND DISCUSSION

Model System. In this study, we first evaluated pairs of double-helical tiles (DAE Tile A + Tile B; D, double-crossover; A, antiparallel; E, even number of half-turns between crossovers)[25] with two, 5-nt SEs extended from the sides of the tiles. The SEs on Tile A are designed to fully hybridize to complementary SEs displayed from Tile B to form a double-helical dimer associated though both SEs (Figure 1). The designs of the double helical tiles were adapted from a previous report,[26] except that a deliberate sequence change was made to the SE region on Tile A, adjacent to the reporter fluorophore (6-FAM), to obtain an optimal signal-to-noise ratio. The sequence of this SE was "Tile A core-TGAGC-5′" (for full sequence details please see the Supporting Information). Here, one thymine residue was placed directly across from the reporter dye to minimize quenching of the fluorophore,[27] and one guanine residue was introduced next to the thymine to suppress the emission of the fluorophore when Tile A alone was present. In that case, the unpaired guanine in the single-stranded region of the tile interacts with the fluorophore (likely through hydrophobic interactions) and quenches its emission *via* a photoinduced electron transfer mechanism.[27,28] Upon full hybridization between the SEs of Tiles A and B, the guanine forms a base pair with a cytosine from the complementary SE and cannot interact with the fluorophore, yielding a prominent enhancement in the emission of the dye. The remaining three nucleotides in the corresponding SEs were held at an identical 60% GC content.

According to steady-state fluorescent analysis, an approximate 40% enhancement and a 3 nm blue shift (from 521 to 518 nm) in the emission of the reporter dye were observed upon dimerization of Tiles A and B (Figure 2a), indicating that after dimerization the reporter was in a more polar environment and subject to fewer quenching factors, such as hydrophobic stacking

and photoinduced electron transfer. These effects are supported by the fluorescence anisotropy measurements (Figure 2b), where a decrease in anisotropy indicates a more free rotation of the dye in the DNA tile dimer.[19] Therefore, we conclude that when the corresponding SE on Tile A is fully hybridized to its complement from Tile B, the fluorophore is "squeezed out" from its stacked position with the neighboring bases on the ssDNA, and thus yields higher fluorescence. The enhancement in fluorescence intensity occurs as hybridization proceeds, thus its time dependence reports the kinetics of DNA tile dimerization.

Kinetics Measurements. Dimerization is initialized by the nucleation of a few base pairs between complementary SEs, and is followed by a rapid "zipping-up" of the remaining complementary base pairs.[15] Nucleation is regarded as the "rate-limiting step" of hybridization at low DNA concentrations,[19] which depends on the accessibility of the nucleation sites and the frequency of successful collisions. The "zipping" step is relatively fast compared to nucleation when fully complementary strands are involved. The most significant change in fluorescence intensity should occur during the "zipping" step. Therefore, the dimerization process can be modeled by a bimolecular association of two separate DNA tile monomers. The free energy change (ΔG) of the tile−tile association reaction between two 5-nt SEs at 25 °C is -14.5 ± 0.1 kcal/mol,[26,29] which indicates that the dimerization equilibrium is strongly dominated by the forward reaction; *i.e.*, once the monomers dimerize, there's little chance for the dimer to dissociate. Thus, the backward dissociation of the dimer can be neglected, and the reaction rate can be expressed as a product of the bimolecular reaction rate constant, k_1, and the concentrations of Tiles A and B (details in the Supporting Information). When the same initial concentration of the tiles is used, the reaction rate can be expressed as a simple second-order reaction: rate = $k_1[A]^2$. The rate constant can be directly obtained from a nonlinear fitting of the plot of fluorescent emission *versus* time (Figure 3a).

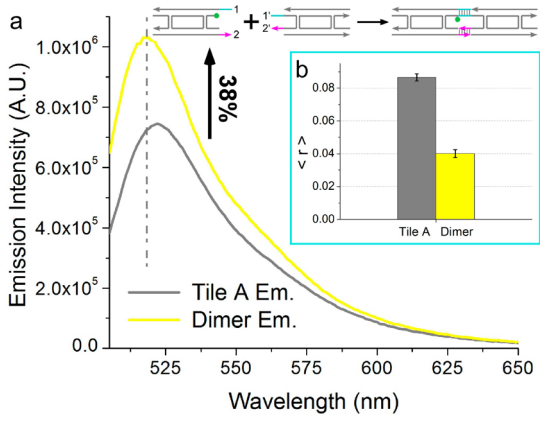

Figure 2. Emission spectra and anisotropy change of the fluorescence of the reporter dye upon tile dimerization. (a) Emission spectra of reporter dye before and after dimerization. A 38% enhancement in the emission intensity, and a 3 nm blue shift of the emission peak were observed after dimerization. (b) Static fluorescence anisotropy measurement before and after dimerization. A decrease in the fluorescence anisotropy value (from 0.086 to 0.040) after dimerization indicates a less restricted rotation of the reporter dye after hybridization of the SEs.

For 5-nt bivalent homodimerization of DAE tiles at 21 °C (room temperature), the second-order rate constant was determined to be $(2.23 \pm 0.07) \times 10^6\ M^{-1}\cdot s^{-1}$. This rate constant is approximately 2-fold higher than the reported rate constant of 20 bp DNA hybridization.[19] When the reporter position was varied (and either of the SEs was monitored) and the direction of the SE pairs was reversed (displayed from the 5′ end of the ssDNA to the 3′ end), the tile−tile dimerization rate constant stayed the same (Figure S22). This result indicates that the kinetics of hybridization does not depend on the orientation of the SEs. This also confirms the reliability of our labeling strategy and accuracy of the corresponding kinetic measurements.

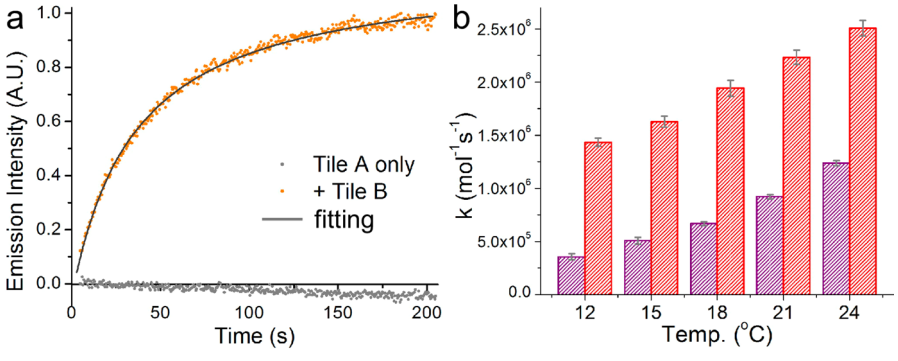

Figure 3. Nonlinear fitting of the second-order reaction. (a) The fluorescence intensity change was normalized from 0 to 1 and corrected for photobleaching using the signal from Tile A only. The graph shown here corresponds to the DAE tile homodimerization (5-nt bivalent). The process was monitored in real time and fit by a second-order reaction equation, from which the rate constant of dimerization was derived. (b) Rate constants of dimerization derived for two samples: DAE homodimers *via* 5-nt bivalent binding (red) and 10-nt monovalent binding (purple). The result indicates that the monovalent binding is slower and is more dependent on temperature. Thus, the monovalent binding exhibits higher activation energy than the bivalent binding.

Compared to ssDNA hybridization kinetics,[18,19] the 2-fold increase in the rate constant of DNA tile dimerization might come from the increased chance of nucleation afforded by the two pairs of SEs. However, it should be noted that, since the total number of bases participating in these two binding processes are not the same, we cannot directly compare the two data sets.

Comparison of Monovalent *vs* Bivalent SE Association. To obtain a more quantitative comparison of mono- and bivalent SE binding, the dimerization kinetics of another pair of DAE tiles was studied. Here, each tile displayed a single 10-nt SE (Tile A core-TGAGC ACACG-5′; 5′-ACTCG TGTGC-Tile B core). The core sequences of the mono- and bivalent pairs of tiles were identical, ensuring that any difference in the binding rate constants arose solely from the unique arrangement of the SEs. The kinetics was measured at 5 different temperatures (Figure 3b). The bivalent binding reaction showed distinctly higher rate constants than the monovalent reaction in all temperatures used in our experiment, indicating that the association rate between the DNA tiles is enhanced by breaking the single 10-nt SE into two 5-nt SEs. However, the rate constant for the single SE interaction shows steeper temperature dependence than that of the bivalent interaction, resulting in a 4-fold difference at 12 °C, and a 2-fold difference at 24 °C.

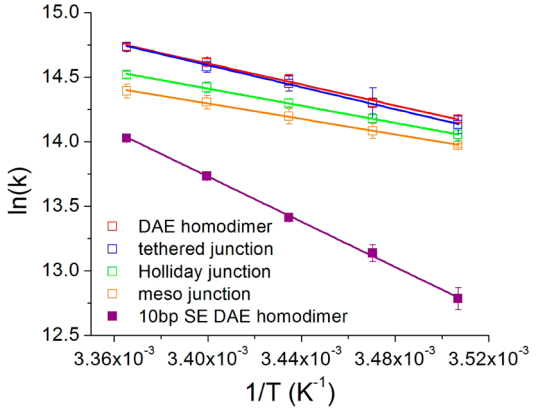

Figure 4. Arrhenius plot of all the tile pairs employed in this study. Rate constants were measured at 5 different temperatures. All tile pairs exhibited a linear relationship between ln *k* and the reciprocal of absolute temperature, 1/*T*. The error bars represent the standard deviation of at least 8 replicate measurements. The error bars are not shown when they are smaller than the size of the symbol used. The activation energy and pre-exponential factor are obtained from the slope and the *y*-intercept of the plot, respectively, and are listed in Table 1.

The activation energies for the dimerization of the different dimers were obtained from the Arrhenius plots (Figure 4 and Table 1). The activation energy of the homodimer of DAE tiles *via* a single 10-nt SE was 17.4 ± 0.4 kcal/mol, close to the previously reported activation energy (~19 kcal/mol) of binding of a 20-nt ssDNA to a multihelix tile.[19] However, the activation energy of the homodimer of DAE tiles *via* two 5-nt SEs is less than half of this value (8.2 ± 0.3 kcal/mol). We should note that a single 5-nt SE interaction between the DAE tiles is not stable, with a melting temperature slightly below room temperature (Figure S17), and thus the dimerization reaction between DAE tiles with a single 5-nt SE does not proceed significantly at room temperature and results in a negligible reaction rate.

From these observations, we conclude that tile−tile association *via* double SEs is beneficial, especially for kinetics. It enhances both the association kinetics and stability compared to the single SEs of the same length. This is because doubling the number of binding sites increases the frequency of nucleation and added base-pairing enhances the binding strength. Compared to a single SE (Figure S19) that is twice as long,[26] the melting temperature of the dimer with two 5-nt SEs is slightly lower than that of the dimer with a single 10-nt SE. The slight destabilization is most likely due to the presence of a few more nick points which weakens the base stacking interactions. However, the kinetics of the tile−tile association *via* two SEs is faster because of an increase in the nucleation frequency and a significant decrease in the activation energy of binding. It seems that the two SEs work cooperatively, such that the nucleation of one of the SEs with its complement helps to bring the neighboring SE with its complement closer together so that alignment occurs before dissociation of the tiles, thus significantly improving the success rate of productive tile−tile association.

Effects of Flexibility of the Double Helical Domains on Kinetics. It is known that in DAE homodimers, the distance between adjacent intra- and intertile double-crossover points are equal to an even number of helical half-turns (21 bps), thus producing nearly planar structures.[30] The existence of multiple double-crossovers in DAE tiles restricts their flexibility, making them approximately twice as stiff along the helical axis as double-stranded DNA molecules of the same length.[31−33] In the individual tiles, both of the SEs are well aligned and brought into close proximity of each other. After mixing, as nucleation of ssDNA domains

TABLE 1. Arrhenius Fitting Results of All the Tile Pairs Investigated in This Study

	DAE homodimer	tethered-junction heterodimer	Holliday-junction heterodimer	meso-junction heterodimer	10-bp SE DAE homodimer
E_a (kcal/mol)	8.1 ± 0.3	8.5 ± 0.2	6.6 ± 0.1	5.9 ± 0.2	17.4 ± 0.4
ln*A*	28.6 ± 0.5	29.1 ± 0.3	25.7 ± 0.2	24.4 ± 0.3	43.5 ± 0.7

occurs between one pair of SEs, there is little additional energy required for the second pair of SEs to align and pair up, and the tile−tile dimerization should proceed with little or no reconfiguration energy costs.

Considering the sequence at the junction position, there is evidence that the HJ tile employed in this study has strong bias toward one stacking conformer,[34] illustrated in the Supporting Information (Figure S2). Therefore, the enthalpic cost of bringing the second SE into close proximity of the first (reconfiguration cost) is also small.[35] However, structural distortion of the SEs will increase the entropic cost of binding, thus resulting in a lower rate of dimerization.

We observe that, for the same length, orientation, and sequence of the SEs, a Holliday-junction Tile B binds to a DAE Tile A to form a heterodimer (Figure 1c) with a rate constant of $(1.83 \pm 0.07) \times 10^6\ M^{-1}\cdot s^{-1}$ at room temperature (21 °C), approximately 18% slower than that of the DAE homodimer (data compiled in Table S3.).

To further investigate the influence of tile flexibility on kinetics, modifications were made to the Holliday-junction tile to increase or restrict its conformation flexibility. In the meso-junction tile (Figure 1d), one crossover is transferred from the reciprocal junction in the center of the tile to the edge of the tile, such that the two helical domains are not as well aligned. We found that the rate constant of heterodimer formation of meso-junction Tile B with DAE Tile A was $(1.63 \pm 0.08) \times 10^6\ M^{-1}\cdot s^{-1}$.

To form a tethered-junction tile, an 8-thymine linker was inserted between the blunt ends of Holliday-junction tile (Figure 1b), making the junction less flexible. The rate constant of dimerization between tethered-junction Tile B and DAE Tile A was measured as $(2.15 \pm 0.09) \times 10^6\ M^{-1}\cdot s^{-1}$ (essentially the same as the DAE homodimer at room temperature, data shown in Table S3).

For all the dimers formed here, the rate constants were determined over a range of temperatures, from 12 to 24 °C. All samples showed a decrease in the rate of dimerization as the temperature decreased, indicating the existence of positive activation energies (Figure 4, Table S3). On the basis of the Arrhenius equation ($\ln(\text{Rate}) = \ln A - E_a/RT$), two factors determine the rate constant: the activation energy (E_a), which is the free energy difference between a high energy transition state and the initial state of the free monomers, and the pre-exponential factor (A), which is related to the probability of collision and the entropic change of the transition.[36] The rate constant is directly proportional to the pre-exponential factor, but exponentially decreases with activation energy.

We speculate that the energy barrier of activation is the result of tile distortion and some weak interactions between the two SEs on the same monomer before dimer formation. Further, the two ends of the flexible junctions rotate over a wider range of angles than the more rigid ones; only when both SEs are properly aligned is synergetic binding allowed to push dimerization toward the forward association reaction. On the basis of this argument, higher flexibility in the tiles is expected to reduce the possibility of successful collisions, thus yielding a lower pre-exponential factor.

Arrhenius plots were generated to obtain the activation energy and pre-exponential factor of dimerization for five different scenarios (Figure 4). We discovered that tiles with higher rigidity have higher activation energies, while at the same time also display higher pre-exponential factors. The two factors affect the rate constant in opposite ways, thus compensating for each other. Here, in the temperature range considered, the pre-exponential factor is the dominating factor of the kinetics of the reaction because the activation energies vary only slightly (6−8 kcal/mol). Note that the highly rigid tiles display two well-aligned SEs for binding, thus they have a higher frequency of successful collisions. However, two closely spaced ssDNA SEs may have weak, transient interactions with each other that must be unraveled before binding with their respective complementary SEs. We speculate that this gives rise to the higher activation energies that were observed.

On the other hand, the flexible tiles generally contain two helical domains twisted relative to each other that act somewhat independently, and so the binding process can be roughly separated into three distinct steps: (1) binding between one pair of the complementary SEs (no preference as to which binds first), (2) reconfiguration of the double helical domain to align the second pair of SEs, and (3) association of the second SE pair before dissociation of the bound one. The activation energies of the three steps likely do not accumulate (perhaps the tile reconfiguration process dominates) thus resulting in lower overall activation energy. At the same time, this also severely decreases the rate of successful collisions. Therefore, we conclude that the binding kinetics of bivalent DNA tile pairs is determined mainly by entropic factors, *i.e.*, successful collisions.

CONCLUSIONS

In this report, we used a fluorescent dye labeled DNA nanostructure to monitor the kinetics of mono- and multivalent DNA tile dimerization. By fitting the kinetics curves, we extracted the rate constants for a series of tile dimers, including DAE homodimers, a DAE/Holliday-junction heterodimer, a DAE/meso-junction heterodimer, and a DAE/tethered-junction heterodimer. The dependence of the tile-dimerization kinetics on many structural factors including dye labeling strategy, construction of the SEs, orientation of the SE binding sites, and the flexibility of double helical domains was studied.

Compared to the kinetics of ssDNA hybridization, the second-order rate constant of DAE homodimer

formation is 2-fold higher, regardless of the fact that DNA tiles are much larger and bulkier than ssDNAs. It appears that the slower translational and rotational diffusion caused by the bulkier DNA tiles does not significantly affect the rate of tile−tile association (Figure S23 and Table S5). This result suggests that increasing the number of SEs increases the nucleation efficiency, thus increasing the rate constant of association.

Employing multiple SEs is a common practice to increase the stability and fidelity of tile−tile assembly. Our study confirms that using two SEs to link DNA tiles enhances the rate of association compared to a single SE with the same number of base pairs. The higher rate is largely because of lower activation energy of dimerization when a single long SE is divided into two shorter ones.

Dimerization of flexible tiles was characterized by lower rate constants than rigid tiles of similar size. Arrhenius plots showed a linear dependence of reaction rate on temperature for all the tile pairs utilized in this study. Increasing the rigidity of the tiles resulted in larger dimerization rate constants. Here there are two factors working in opposition: higher activation energies decrease the rate while much higher preexponential factors dominate and increase the overall rate. Our data predicts that dimerization reactions with lower activation energies will be faster at sufficiently higher temperatures. However, it is important to note that the dimers would melt at those temperatures. Therefore, the temperature range in which DNA tiles can be manipulated is quite narrow: 0 °C < T < T_m, where T_m is the melting temperature of the SEs. For the dimers studied here, the T_m ranges from 30 to 40 °C.[26] Using a higher assembly temperature (lower than T_m) would mitigate the difference between the reaction rates among different structured dimers, while a lower temperature (>0 °C) would make the rates more dissimilar. Depending on the purpose of the assembly and complexity of the tile mixture, optimal temperatures can be identified. For a one-pot annealing reaction, the annealing program can also be adjusted to have different temperature ramps in the different temperature ranges to make the assembly process more efficient and less time-consuming.

Understanding how individual molecular components interact with one another, both in terms of their spatial arrangement and temporal interaction within the larger networks, is of paramount importance to their application. Specifically, design guidelines for elaborate motifs are required to enable the construction of dynamic DNA devices and allow them to perform challenging tasks. We believe that the results presented here will assist in improved implementation of DNA tile based algorithmic self-assembly, DNA based molecular robotics, and other specific nucleic acid systems.

MATERIAL AND METHODS

Self-Assembly of DNA Nanostructures. All DNA strands used for the assembly of nanostructures were purchased from Integrated DNA Technologies, Inc. (www.idtdna.com) and purified by denaturing polyacrylamide gel electrophoresis (PAGE; 8.3 M urea, 6−10% acrylamide in 1× TBE buffer: 89 mM Tris base, 89 mM boric acid, 2 mM EDTA, pH 8.0) for the unmodified DNA oligomers, or by HPLC for the dye-labeled DNA oligomers. The design of DAE double-helical tiles included one oligomer modified with 6-carboxylfluorescein (6-FAM). The tiles were assembled by mixing equimolar amounts of all the oligomers present in the structures at a final concentration of 500 nM, in 1× TAE Mg^{2+} buffer (40 mM Tris base, 20 mM acetic acid, 2 mM $EDTA \cdot Na_2 \cdot 12H_2O$, 12.5 mM $((CH_3COO)_2Mg_3 \cdot 4H_2O)$), then by heating the mixtures at 95 °C and cooling to 4 °C over 2 h using an automated PCR thermocycler (Mastercycler Pro, Eppendorf).

Nondenaturing Gel Electrophoretic Characterization of Nanostructures. The assembly of all tile designs and subsequent dimers were confirmed by nondenaturing polyacrylamide gel electrophoresis. Structures (2.5 pmol of each tile, before and after dimerization) were analyzed by 7% nondenaturing PAGE gels in 1× TAE Mg^{2+} buffer. Electrophoresis was performed at 200 V, 15 °C for 2.5 h. The gels were first analyzed with a Bio-Rad Gel Doc XR+ system with excitation of fluorescein for visualization. The gels were subsequently stained with ethidium bromide (EB) and scanned in a Bio-Rad Gel Doc XR+ system for tile and dimer visualization.

Fluorescence Measurements. All steady-state and real-time fluorescence spectra were measured by a Nanolog fluorometer (Horiba Jobin Yvon, L-format, equipped with a CW 450 W xenon light source, thermoelectrically cooled R928 PMT, and fully automated excitation and emission polarizers for anisotropy measurements), with a 1 cm path length quartz cell (Starna Cells, Inc.). All spectra were corrected for the wavelength dependence of the detection system response. A volume of 120 μL of 20 nM tile solution was used for all measurements. Fluorescence emission spectra were collected using 495 nm excitation, 4 nm excitation slits, 505−650 nm emission wavelength range, 5 nm emission slits, and 0.5 s integration. Fluorescence anisotropy was measured with 495 nm excitation, 4 nm excitation slits, 520 nm emission, 5 nm emission slits, and 0.5 s integration. Anisotropy values were calculated from the instrument software FluorEssence for Windows by Horiba Scientific.

Real-Time Fluorescence Measurements. The kinetics of dimerization of complementary DNA tiles was monitored in real-time *via* changes in the emission of the fluorescence dye reporter that occurred upon DNA hybridization. Unless otherwise noted, 120 μL of 5−20 nM tile solution was used for all measurements. The parameters used to collect real-time spectra are described as follows: 495 nm excitation, 1 nm excitation slits (to avoid photobleaching), 520 nm emission, 15 nm emission slits (to collect maximum signal), and 0.5 s integration. The fluorescent signal of the tile solution was collected for 120−300 s (depending on the concentration and tile species) to confirm the photostability of the fluorophore with continuous exposure to the excitation source. A 1−2% reduction in the overall emission of the equilibrated solutions was observed for a typical measurement period. Next, data collection was initiated in the dark, and an equimolar amount of complementary tile was directly added to the cuvette secured in the instrument. The solution was mixed well by pipetting for 3 s, and the kinetics of hybridization of the binding sites was followed by monitoring the intensity of FAM emission for the extent of the reaction.

Conflict of Interest: The authors declare no competing financial interest.

Acknowledgment. The authors want to acknowledge financial support from NSF, NIH, and DOE to H.Y. and Y.L.

Supporting Information Available: Data analysis, DNA sequences and design details, gel characterization of the individual DNA tiles and dimers, thermodynamic measurements, and additional kinetic measurements. This material is available free of charge *via* the Internet at http://pubs.acs.org.

REFERENCES AND NOTES

1. Seeman, N. C. Nucleic-Acid Junctions and Lattices. *J. Theor. Biol.* **1982**, *99*, 237–247.
2. Rothemund, P. W. K. Folding DNA To Create Nanoscale Shapes and Patterns. *Nature* **2006**, *440*, 297–302.
3. Seeman, N. C. An Overview of Structural DNA Nanotechnology. *Mol. Biotechnol.* **2007**, *37*, 246–257.
4. Aldaye, F. A.; Palmer, A. L.; Sleiman, H. F. Assembling Materials with DNA as the Guide. *Science* **2008**, *321*, 1795–1799.
5. Pinheiro, A. V.; Han, D.; Shih, W. M.; Yan, H. Challenges and Opportunities for Structural DNA Nanotechnology. *Nat. Nanotechnol.* **2011**, *6*, 763–772.
6. Dietz, H.; Douglas, S. M.; Shih, W. M. Folding DNA into Twisted and Curved Nanoscale Shapes. *Science* **2009**, *325*, 725–730.
7. Han, D.; Pal, S.; Nangreave, J.; Deng, Z.; Liu, Y.; Yan, H. DNA Origami with Complex Curvatures in Three-Dimensional Space. *Science* **2011**, *332*, 342–346.
8. Wei, B.; Dai, M.; Yin, P. Complex Shapes Self-Assembled from Single-Stranded DNA Tiles. *Nature* **2012**, *485*, 623–626.
9. Ke, Y.; Ong, L. L.; Shih, W. M.; Yin, P. Three-Dimensional Structures Self-Assembled from DNA Bricks. *Science* **2012**, *338*, 1177–1183.
10. Han, D.; Pal, S.; Yang, Y.; Jiang, S.; Nangreave, J.; Liu, Y.; Yan, H. DNA Gridiron Nanostructures Based on Four-Arm Junctions. *Science* **2013**, *339*, 1412–1415.
11. Gu, H.; Chao, J.; Xiao, S. J.; Seeman, N. C. A Proximity-Based Programmable DNA Nanoscale Assembly Line. *Nature* **2010**, *465*, 202–205.
12. Douglas, S. M.; Bachelet, I.; Church, G. M. A Logic-Gated Nanorobot for Targeted Transport of Molecular Payloads. *Science* **2012**, *335*, 831–834.
13. Qi, H.; Ghodousi, M.; Du, Y.; Grun, C.; Bae, H.; Yin, P.; Khademhosseini, A. DNA-Directed Self-Assembly of Shape-Controlled Hydrogels. *Nat. Commun.* **2013**, *4*, 2275.
14. Craig, M. E.; Crothers, D. M.; Doty, P. Relaxation Kinetics of Dimer Formation by Self Complementary Oligonucleotides. *J. Mol. Biol.* **1971**, *62*, 383–392.
15. Wetmur, J. G. Hybridization and Renaturation Kinetics of Nucleic Acids. *Annu. Rev. Biophys. Bioeng.* **1976**, *5*, 337–361.
16. Wetmur, J. G. DNA Probes: Applications of the Principles of Nucleic Acid Hybridization. *Crit. Rev. Biochem. Mol. Biol.* **1991**, *26*, 227–259.
17. Chen, C.; Wang, W.; Wang, Z.; Wei, F.; Zhao, X. S. Influence of Secondary Structure on Kinetics and Reaction Mechanism of DNA Hybridization. *Nucleic Acids Res.* **2007**, *35*, 2875–2884.
18. Yin, Y.; Zhao, X. S. Kinetics and Dynamics of DNA Hybridization. *Acc. Chem. Res.* **2011**, *44*, 1172–1181.
19. Pinheiro, A. V.; Nangreave, J.; Jiang, S.; Yan, H.; Liu, Y. Steric Crowding and the Kinetics of DNA Hybridization within a DNA Nanostructure System. *ACS Nano* **2012**, *6*, 5521–5530.
20. Ouldridge, T. E.; Sulc, P.; Romano, F.; Doye, J. P. K.; Louis, A. A. DNA Hybridization Kinetics: Zippering, Internal Displacement and Sequence Dependence. *Nucleic Acids Res.* **2013**, *41*, 8886–8895.
21. Rauzan, B.; McMichael, E.; Cave, R.; Sevcik, L. R.; Ostrosky, K.; Whitman, E.; Stegemann, R.; Sinclair, A. L.; Serra, M. J.; Deckert, A. A. Kinetics and Thermodynamics of DNA, RNA, and Hybrid Duplex Formation. *Biochemistry* **2013**, *52*, 765–772.
22. Johnson-Buck, A.; Nangreave, J.; Jiang, S.; Yan, H.; Walter, N. G. Multifactorial Modulation of Binding and Dissociation Kinetics on Two-Dimensional DNA Nanostructures. *Nano Lett.* **2013**, *13*, 2754–2759.
23. Du, S. M.; Zhang, S.; Seeman, N. C. DNA Junctions, Antijunctions, and Mesojunctions. *Biochemistry* **1992**, *31*, 10955–10963.
24. Wang, H.; Seeman, N. C. Structural Domains of DNA Mesojunctions. *Biochemistry* **1995**, *34*, 920–929.
25. Fu, T.; Seeman, N. C. DNA Double-Crossover Molecules. *Biochemistry* **1993**, *32*, 3211–3220.
26. Nangreave, J.; Yan, H.; Liu, Y. DNA Nanostructures as Models for Evaluating the Role of Enthalpy and Entropy in Polyvalent Binding. *J. Am. Chem. Soc.* **2011**, *133*, 4490–4497.
27. Doose, S.; Neuweiler, H.; Sauer, M. Fluorescence Quenching by Photoinduced Electron Transfer: A Reporter for Conformational Dynamics of Macromolecules. *ChemPhysChem* **2009**, *10*, 1389–1398.
28. Torimura, M.; Kurata, S.; Yamada, K.; Yokomaku, T.; Kamagata, Y.; Kanagawa, T.; Kurane, R. Fluorescence-Quenching Phenomenon by Photoinduced Electron Transfer between a Fluorescent Dye and a Nucleotide Base. *Anal. Sci.* **2001**, *17*, 155–160.
29. Nangreave, J.; Yan, H.; Liu, Y. Studies of Thermal Stability of Multivalent DNA Hybridization in a Nanostructured System. *Biophys. J.* **2009**, *97*, 563–571.
30. Arbona, J. M.; Aimé, J. P.; Elezgaray, J. Modeling the Mechanical Properties of DNA Nanostructures. *Phys. Rev. E: Stat., Nonlinear, Soft Matter Phys.* **2012**, *86*, 051912.
31. Li, X.; Yang, X.; Qi, J.; Seeman, N. C. Antiparallel DNA Double Crossover Molecules as Components for Nanoconstruction. *J. Am. Chem. Soc.* **1996**, *118*, 6131–6140.
32. Sa-Ardyen, P.; Vologodskii, A. V.; Seeman, N. C. The Flexibility of DNA Double Crossover Molecules. *Biophys. J.* **2003**, *84*, 3829–3837.
33. Schiffels, D.; Liedl, T.; Fygenson, D. K. Nanoscale Structure and Microscale Stiffness of DNA Nanotubes. *ACS Nano* **2003**, *7*, 6700–6710.
34. Altona, C. Classification of Nucleic Acid Junctions. *J. Mol. Biol.* **1996**, *263*, 568–581.
35. McKinney, S. A.; Déclais, A. C.; Lilley, D. M.; Ha, T. Structural Dynamics of Individual Holliday Junctions. *Nat. Struct. Biol.* **2003**, *10*, 93–97.
36. Laidler, K. J.; King, M. C. Development of Transition-State Theory. *J. Phys. Chem.* **1983**, *87*, 2657–2664.